Golub, M.; Combet, S.; Wieland, D.C.F.; Soloviov, D.; Kuklin, A.;
Lokstein, H.; Schmitt, F.-J.; Olliges, R.; Hecht, M.; Eckert, H.-J.; Pieper, J.:

Solution structure and excitation energy transfer in phycobiliproteins of Acaryochloris marina investigated by small angle scattering

In: Biochimica et Biophysica Acta: Bioenergetics (2017) Elsevier

DOI: 10.1016/j.bbabio.2017.01.010

Low-resolution structure and excitation energy transfer in phycobiliproteins of *Acaryochloris marina* investigated by small angle scattering

M. Golub[a], S. Combet-Jeancenel[b], D. Lairez[b], F. Wieland[c], D. Soloviov[d], A. Kuklin[d], H. Lokstein[e], F.-J. Schmidt[f], M. Hecht[a], H.-J. Eckert[f], and J. Pieper[a]*

[a] *Institute of Physics, University of Tartu, Tartu, Estonia*

[b] *LLB Saclay, France, lairez@llb.saclay.cea.fr*

[c] *DESY, Hamburg, Germany*

[d] *Frank Laboratory, JINR, Dubna, Russia*

[e] *Charles University Prague, Faculty of Mathematics and Physics, Department of Chemical Physics and Optics, Ke Karlovu 3, 121 16 Prague, Czech Republic*

[f] *Max-Volmer-Laboratories for Biophysical Chemistry, Technical University Berlin, Germany*

*Author to whom correspondence should be addressed:

Jörg Pieper

Institute of Physics, University of Tartu, W. Ostwaldi 1, 50411 Tartu, Estonia.

phone.: +(372) 737 4627

fax: +(372) 738 3033

email: pieper@ut.ee

Keywords: Acaryochloris marina, phycobiliproteins, excitation energy transfer, small angle neutron scattering, small angle X-ray scattering,

Abstract

The structure of phycobiliproteins (PBPs) of the cyanobacterium *Acaryochloris marina* was investigated under close-to-native conditions in buffer solutions containing and lacking phosphate, respectively, using small angle neutron scattering (SANS) at physiological temperatures. The scattering data of intact PBPs can be well described using a cylindrical shape with a length of about 225 Å and a diameter of roughly 100 Å. This finding is qualitatively consistent with earlier electron microscopy studies reporting a rod-like PBP shape with a length of about 250 (M. Chen et al., FEBS Letters 583, 2009, 2535) or 300 Å (J. Marquart et al., FEBS Letters 410, 1997, 428). In contrast, PBPs dissolved in MES-buffer lacking phosphate revealed a splitting of the PBP rods into cylindrical subunits with a remaining height of 28 Å only, but also a pronounced sample aggregation. Complementary SANS and small angle X-ray scattering (SAXS) experiments on phycocyanin (PC) suggest that the cylindrical subunits may be identical to trimeric PC, while trimeric APC would produce roughly the same low-resolution structure. The latter finding is in agreement with the assumption that a PBP-rod with a total length of about 225 Å can accommodate 7 trimeric PC and one APC subunits, each of which have a length of about 28 Å. The structural information can be used to interpret variations in the low-energy region of the 4.5 K absorption spectra of PBPs dissolved in buffer solutions containing and lacking phosphate, respectively.

List of Abbreviations

APC - allophycocyanin

Chl - Chlorophyll

EET excitation energy transfer

FLN – fluorescence line-narrowing

ΔFLN – difference fluorescence line-narrowing

FWHM – full width at half maximum

PC - phycocyanin

PBP - phycobiliprotein

PBS – phycobilisomes

PCB - phycocyanobilin

PE - phycoerythrin

RC - reaction center

SANS – small angle neutron scattering

SAXS – small angle X-ray scattering

1. Introduction

The cyanobacterium *Acaryochloris marina* (*A.marina*) is characterized by using Chlorophyll (Chl) *d* as the major photosynthetic pigment [1]. *A.marina* (strain MBIC 11017) features a light-harvesting system consisting of core complexes referred to as CP43/CP47, membrane intrinsic Chl *d* containing proteins [2, 3] and membrane extrinsic phycobiliprotein (PBP) complexes [4, 5]. PBP complexes contain phycocyanin (PC) and allophycocyanin (APC) and exhibit a broad absorption spectrum at about 618 nm at room temperature, which allows to utilize visible light between 500 nm and 650 nm that is out of the accessible absorption range of Chls [4, 5].

So far, direct information on the structure of PBPs of *A.marina* is rather scarce. PBPs are equivalent to the phycobilisomes (PBS) of Chl *a*-binding cyanobacteria. The latter are usually composed of an APC-containing core and of rod-like structures containing either PC-hexamers or both PC- and phycoerythrin (PE) - hexamers (see [6,7,8] for reviews). In contrast, cryo-electron microscopy studies revealed that PBPs are organized in individual rods containing four hexameric subunits in the case of *A.marina* [9, 10]. Each PBP rod was inferred to consist of three homo-hexamers of PC and an additional hetero-hexamer containing PC and APC [4]. The latter arrangement was verified by Theiss et al. [11] for the PBP preparation used in the present study.

Transient absorption experiments [11, 12] were used to investigate the dynamics of excitation energy transfer (EET) in the PBP antenna of *A.marina* on femtosecond (fs) resolution. Excitation at 618 nm led to ultrafast EET from ~620 nm to ~630 nm subsequently followed by slower EET to states at ~640 nm and further to the terminal emitter at ~670 nm at room temperature. Eventually, the excitation energy seems to be directly funnelled from the terminal emitter of

PBPs to the Chl *d*–containing reaction center of PS II [5, 11]. These results were recently summarized by Theiss et al. [13]. Fluorescence line-narrowing (FLN) and difference fluorescence line-narrowing (ΔFLN) at 4.5 K [14] were used to identify up to five low-energy electronic states involved in the above ultrafast EET dynamics, their inhomogeneous broadening and electron-phonon coupling parameters. In more detail, the electronic states at ~633 and 644 nm was tentatively attributed to PC and APC, respectively, while the terminal emitter was found at 673 nm. Fluorescence studies revealed that EET is intact in PBPs in phosphate-containing buffer, but impaired when PBPs are dissolved in phosphate-less buffer (see [13] and references therein). Based on this finding it was inferred that PBPs in phosphate-less buffer may be split into individual subunits, however, there is no direct structural information.

In this regard, small-angle neutron and X-ray scattering (SANS and SAXS, respectively) are valuable experimental techniques providing low-resolution structural information in close-to-native aqueous environments (for reviews, see [15, 16]). SANS and SAXS have also been successfully employed in photosynthesis research [17]. For example, neutron studies of plant thylakoid membranes have revealed a size of the grana unit cell of 157 Å in solution [18, 19], the hydration dependence of the PS II membrane spacing [20], but also the structural arrangement of cyanobacterial thylakoid membranes [21]. In addition, SANS was also used to determine the structure of plant antenna complex LHC II [22] and bacterial light-harvesting complex LH2 in buffer solution at physiological temperatures [23].

In the present study, we apply SANS and SAXS for structural investigation of PBPs of *A. marina* under close-to-native conditions in buffer solutions containing and lacking phosphate, respectively, at physiological temperatures. The results obtained are used to explain differences in the low-energy level structure of PBPs observed by absorption spectroscopy.

2. Materials and Methods

Sample Preparation:

***PBP from A. marina*:** The preparation of the PBP samples of *A. marina* used in the present study was described in detail in Gryliuk et al. [14]. Briefly, cells of *A. marina* (MBIC-11017) were grown in artificial sea water according to [24]. Phycobiliproteins were isolated by density gradient centrifugation as described before by Marquardt et al. [4]. Finally, the samples were dissolved in two different buffer solutions containing or lacking phosphate, hereafter referred to as +P and –P-buffer, respectively. The +P buffer was composed of 0.375 M K_2HPO_4, 0.375 M KH_2PO_4, 10% (w/v) sucrose, and 2 µM EDTA at pH 7.0. In contrast, the phosphate-less –P buffer contained 10 mM MES, 10% (w/v) sucrose, and 2 µM EDTA at pH 7.0. For SANS experiments, the samples were transferred to D_2O-containing buffers with pD 7.0.

Phycocyanin from T. elongatus: Cells were harvested by centrifugation and the pellet was resuspended in 20 mM Tricin-buffer (pH 7.8). Cells were broken in a French press at 950 PSI and ultracentrifuged for 10 min at 30.000 rpm. The blue supernatant was concentrated in Centricon 100 devices and further purified by ultracentrifugation on a sucrose gradient at 30.000 rpm for 16 h (overnight) at 4 °C. The blue C-PC band was recovered and concentrated as above to reach a final protein concentration of 10 mg/ml.

Small Angle Neutron and X-ray Scattering:

The SANS experiments on PBP +P and –P were carried out at the instrument PACE at the LLB Saclay (France). Three configurations were used employing incident neutron wavelengths/sample-detector distances of 12 Å/4.7 m, 6 Å/3 m, and 4.5 Å/1 m, respectively, in order to probe a wide Q-range of 0.007 to 0.8 $Å^{-1}$. The data were corrected as described in [25].

The SANS experiments on PC were performed at the small angle time-of-flight instrument YuMO in the Frank Laboratory of Neutron Physics (FLNP) of the Joint Institute for Nuclear Research (JINR) in Dubna, Russia. The wavelength range of the incident neutron beam used in the experiment was about 0.5-8 Å. The sample-to-detector distance was set to 18 m, which allowed the collection of data in the Q range from 0.0063 $Å^{-1}$ to 0.58 $Å^{-1}$. Each data set was collected for 5 hours of measurement time to achieve sufficient statistics. The PC samples were placed into 1 mm thick quartz cuvettes. A contrast variation experiment was carried out using two buffer solutions containing 5% and 100% D_2O, respectively.

The SAXS experiments on PC were carried out using the NanoStar SAXS instrument (Brucker AXS GmbH, Karlsruhe, Germany) at DESY Hamburg, Germany, where an X-ray beam with a wavelength of 1.54 Å is provided by a copper lamp. The data were collected by a VANTEC 2000 detector (14x14 cm in size, resolution of 2048x2048 pixels) at a sample-to-detector distance of 103 cm. To exclude the protein-protein interaction the concentration of the protein was reduced to 5, 2.5 and 1.3 mg/ml. The samples were placed into glass capillary vessels with a diameter of 2 mm. The data treatment took into account the scattering from the solvent and capillary, detector efficiency and background signal. The data corrections were carried out using the Fit2D program developed at ESRF.

Data analysis

The small angle scattering from a diluted solution of monodisperse particles follows the master formula [15,16]

$$\frac{d\sigma(q)}{d\Omega(q)} = n\Delta\rho^2V^2P(q)S(q) \quad \frac{d\sigma(q)}{d\Omega(q)} = n\Delta\rho^2V^2P(q)S(q), \qquad (1)$$

where n is the number of particles, Δρ is the difference in scattering length densities between the particles and the solvent, and V is the volume of the particles. P(q) is the form factor, which is a function of the averaged shape and the averaged size of the scattering particles. The effective structure factor is presented in the formula as S(q), which is equal to unity for diluted solutions without interaction between the individual particles.

The radius of gyration R_g for the experimental scattering curves was evaluated according to the classical Guinier approximation:

$$I(q) = I(0) \exp\left(-q^2 \frac{Rg^2}{3}\right), \quad (2)$$

which is valid for small q values according to $qR_g<<3$. Here, I(0) is the forward scattering, which is a shape independent function of the total scattering power of the sample. The distance distribution function P(R) and particle maximum dimension D_{max} were determined by fitting the data using the indirect Fourier transform (IFT) method as implemented in the program GNOM [26].

In case of partial aggregation, the SANS data were fitted using a linear superposition of two intensity profiles: a) the scattering profile of a cylinder with uniform scattering length density corresponding to the PC subunit, and b) a power law mimicing the scattering of aggregates. The global fitting of SANS curves was performed using the NSNR SANS software developed at NIST [27].

The form factor of a monodisperse circular cylinder with uniform scattering length density is normalized by the particle volume V_{cyl} and averaged over all possible orientations of the cylinder according to

$$P(q) = \frac{s}{V_{cyl}} \int_0^{\frac{\pi}{2}} f^2(q,\alpha) \sin(\alpha) d\alpha \qquad (3)$$

with

$$f(q,\alpha) = 2\Delta\rho V_{cyl} j_0\left[\frac{qL\cos(\alpha)}{2}\right] \frac{j_1[qr\sin(\alpha)]}{qr\sin(\alpha)}, \qquad (4)$$

where s is a scaling factor, α is the angle between the cylinder axis and the scattering vector q, r is the radius, and L the length of the cylinder. The integral over alpha averages the form factor over all possible orientations of the cylinder with respect to q. Furthermore, $j_0(x)$ and $j_1(x)$ are the zero- and first-order Bessel functions with $j_0(x)$ being

$$j_0(x) = \frac{\sin(x)}{x} \qquad (5)$$

and the cylinder volume given by

$$V_{cyl} = \pi r^2 L. \qquad (6)$$

The structure of PC in solution was obtained using the ATSAS reconstitutions tools, which was developed by the group of Dmitri Svergun based on a reverse Monte Carlo minimization approach [28, 29]. The ab structure models of PC derived within this study are sphere structures averaged over 20 iterations; for each iteration it was taken into account that the PC subunit has an oblate disk like shape with a P_3 symmetry. We have also applied the Crysol program [30] in order to calculated a theoretical SAXS curve based on the pdb structure of PC in hexameric and trimeric forms with the experimental SAXS data.

RESULTS AND DISCUSSION

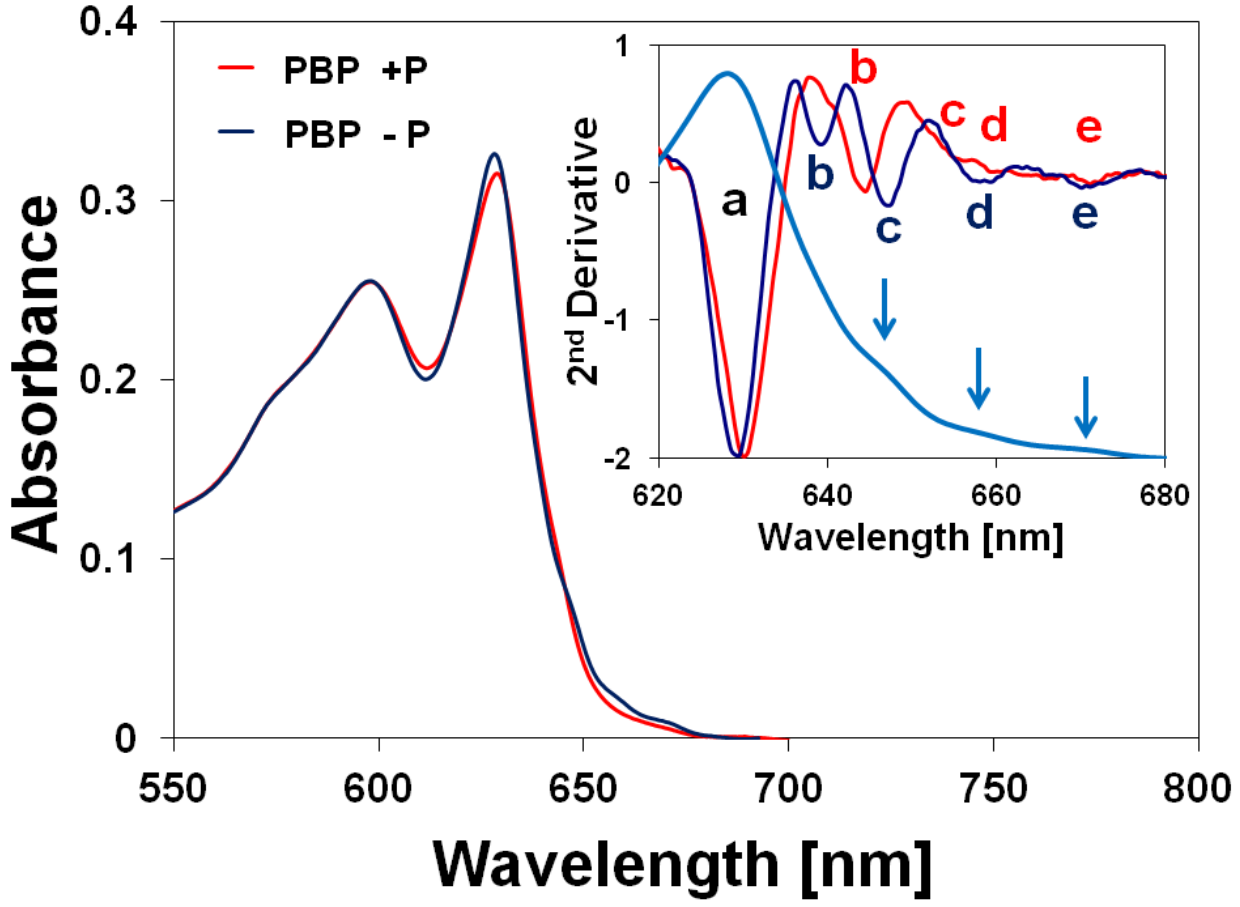

Figure 1. Absorption spectra of PBPs of *A.marina* dissolved in buffers containing (red line) or lacking phosphate (blue line), respectively, measured at 4.5 K. The inset shows the second derivatives of the absorption spectra in the low-energy region applying the same color code. Minima of the second derivative spectra are labeled, see text. For comparison the 4.5 K absorption spectrum of PBPs of *A.marina* without phosphate is shown as a light blue line.

The 4.5 K absorption spectra of PBPs of *A.marina* dissolved in buffer solutions containing or lacking phosphate, respectively, are shown in Fig. 1. In what follows the two PBP forms will be referred to as PBP +P and PBP -P, respectively. The two absorption spectra seen in Fig. 1 are widely identical, but exhibit slight differences in the low-energy region. The latter differences are better visible in the second derivative spectra shown in the inset of Fig. 1, where the minima in

the two spectra are labeled by small letters a – e for the cases of PBP +P (red) and PBP –P (blue), respectively. The 4.5 K absorption spectrum of PBP +P is virtually identical to that published before by Gryliuk et al. [14] with a major peak at ~629 nm (a) and further minima in the second derivative spectrum at ~644 nm (b), ~654 nm (c), ~659 nm (d), and ~673 nm (e). All these structures coincide very well with low-energy electronic states assigned by Gryliuk et al. [14] based on difference fluorescence line-narrowing spectroscopy. Upon phosphate removal, the major peak of the PBP –P spectrum seems to shift to the blue by about 2 nm. Instead of the former peak b, there appear to be two minima in the PBP –P spectrum at ~639 and ~647 nm, respectively. The less intense peaks c and d seem to merge into the broad minimum d at ~658 nm in the PBP –P spectrum. The minimum e at ~673 nm attributed to the terminal emitter [13, 14] is too shallow to conclude about any effect of phosphate removal in this case. The changes in the low-energy electronic structure of PBPs upon phosphate removal are also reflected in the appearance of more pronounced peaks in the absorption spectrum of PBP –P, which are labeled by arrows in the inset of Fig. 1, but especially of the peak at ~645 nm previously assigned to APC [14]. Most generally, these effects can be explained by a number of different effects: a) alteration of the protein environment of the pigment molecules concerned, b) changes in excitonic coupling between pigment molecules, or c) effects due to aggregation. It was observed before, that in PBP –P samples EET from the PC/APC electronic states to the terminal emitter is impaired (see [13] and references therein). Therefore, it was inferred that phosphate removal may affect the structural integrity of the PBP rods. In what follows, we will report on SANS and SAXS studies of PBP +P and PBP –P as well as on PC subunits which probe the possible structural alteration due to phosphate removal.

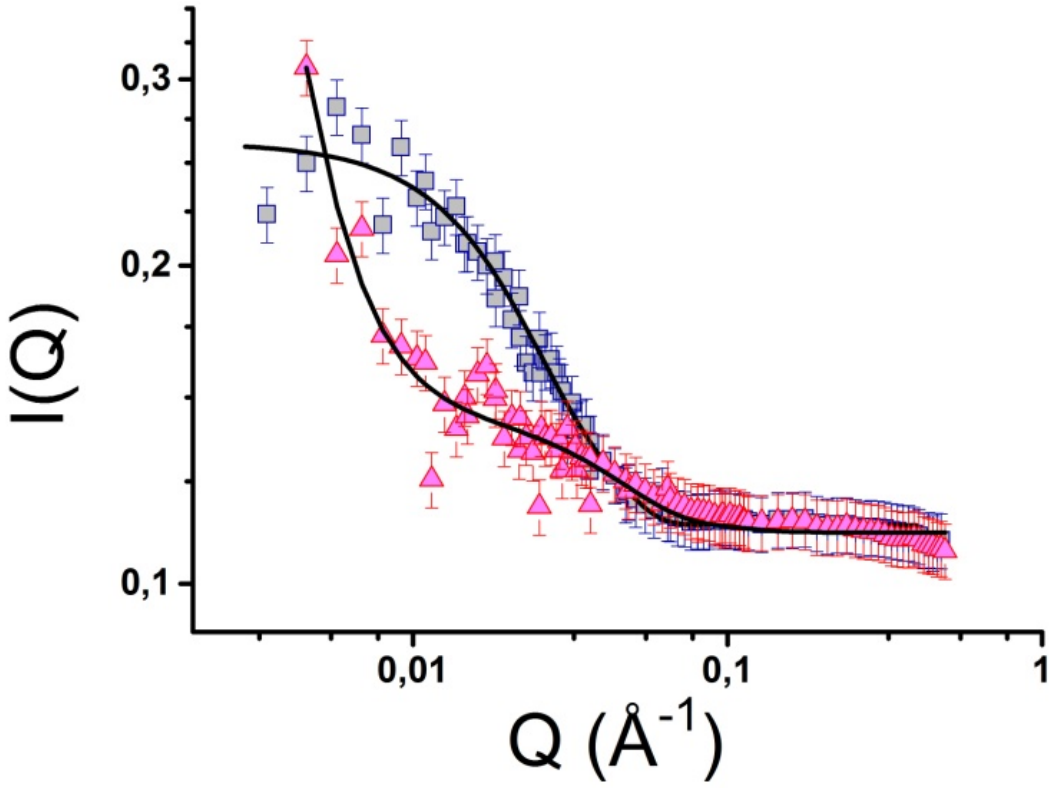

Figure 2. SANS data of PBPs of *A.marina*, which are dissolved in buffers containing (PBP +P, blue squares) or lacking phosphate (PBP –P, red triangles), respectively, measured using the instrument PACE at room temperature. The full black lines are simultaneous fits of both data sets (see Table 1 for parameters).

SANS data of PBP +P and PBP –P of *A.marina* measured using the instrument PACE at room temperature are shown in Fig. 2. As expected based on previous studies [4, 10, 13], the data can be well approximated using the model of a monodisperse circular cylinder with a radius of 50±5 Å and a length of 225±20 Å, see Table 1 for parameters. This finding confirms the rod-shaped structure, but also the approximate dimensions of the PBP rods reported from different electron microscopy studies [4, 10, 13]. However, the SANS data presented here were obtained in buffer solution at room temperature and represents the bulk sample. Thus, SANS data are measured under more native conditions than applied for electron microscopy, because the latter technique requires staining and/or fixation of the samples.

A comparison of the PBP +P data with those obtained for PBP –P reveals that the signal due to the cylindric shape is strongly decreased, while a strongly increasing signal is observed towards lower scattering vectors Q. The latter is most likely the signature of pronounced aggregation in PBP –P samples. Keeping in mind that a split up of the PBP rods upon phosphate removal was inferred before [13], the PBP –P data were fitted with a model comprising a monodisperse circular cylinder with a radius of 50±5 Å and a power law to describe possible aggregates. A satisfactory fit of the data can be achieved for a circular cylinder with a height of 28±5 Å, see Fig. 2 and Table 1 for the complete parameter set. This suggests that upon phosphate depletion, the PBP rods split into smaller disk-shaped subunits with a height of approximately 30 Å, while a relatively large share of them forms large, unspecific aggregates.

The latter results do not yet allow for an unambiguous identification of the PBP subunits present in the PBP –P samples. Therefore, we performed additional SANS and SAXS experiments using PC from *Th. elongatus* assuming a strong structural homology between PC of *Th. elongatus* and *A.marina*, respectively. The PC structure was first investigated using SANS at the YuMO instrument applying different contrasts of 5% and 100% D_2O, respectively, see Fig. 3. The full lines in Fig. 3 are the result of a simultaneous fit of both data sets with the same model function applied before to the PBP –P data, i.e. a circular cylinder plus a power law accounting for slight aggregation occurring at the relatively high protein concentration employed. The fit parameters listed in Table 1 reveal that also the SANS data of PC can be fitted using cylindrical shapes with a radius of 50±5 Å and a height of 28±5 Å as obtained before for PBP –P. This result suggests that upon phosphate removal, the PBP rods are split in subunits of similar size as the PC complexes investigated within this study.

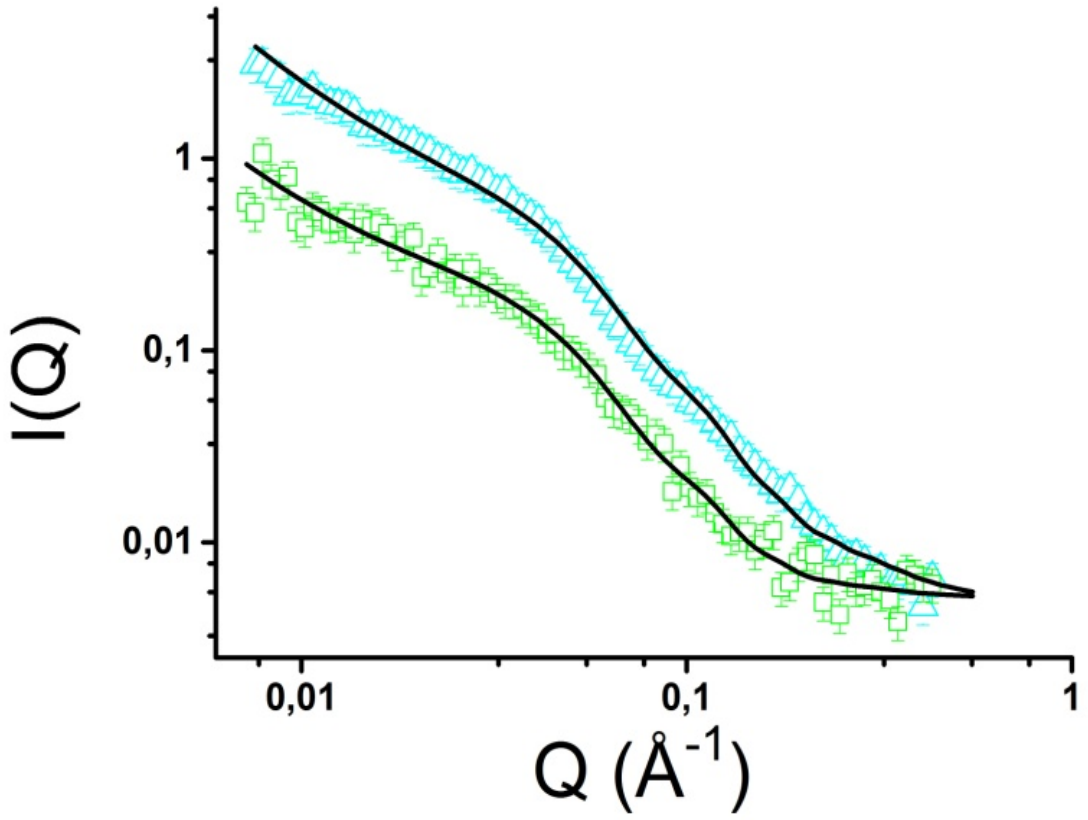

Figure 3. SANS data of PC of *Th.elongatus* measured at a protein concentration of 10 mg/ml at contrasts of 100% D_2O (blue triangles) and 5% D_2O (green squares), respectively, using the instrument YUMO at room temperature. The full black lines are simultaneous fits of both data sets (see Table 1 for parameters).

Further SAXS data of PC of *Th. elongatus* obtained on Nanostar at room temperature are shown in Panel A of Fig. 4. The pair distance distribution function P(R) derived from the SAXS data by indirect Fourier transform using the program GNOM is shown Panel B of Fig. 4. The full black and red lines in Panel A are fits of the SAXS data generated from the trimeric and hexameric PC structure (see [31], pdb code 4L1E) using the CRYSOL program. It is apparent that the data can be very well described by the trimeric form of PC, while the the hexameric structure seems to be too large to provide an acceptable fit. It has to be added that the SAXS data can be fitted by the same cylindrical model applied before to the PC SANS data (not shown), however, no component due to aggregation is necessary.

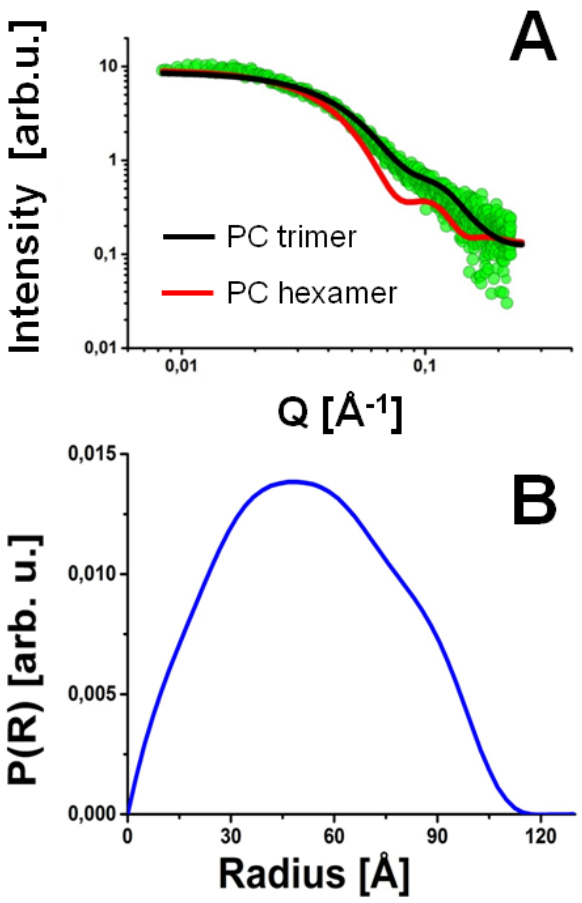

Figure 4. Panel A: SAXS data of PC of *Th.elongatus* obtained on Nanostar (green circles) at room temperature. The full black and red lines are fits assuming trimeric and hexameric PC structure, see also Fig. 5. Panel B: Pair correlation function P(R) derived from the SAXS data shown in Panel A.

Finally, an ab initio shape reconstitution of PC was carried out using the reverse Monte Carlo minimization approach of the ATSAS routine. The resulting low-resolution model of PC is shown in grey in Fig. 5 and compared to the high-resolution X-ray structure of PC. It is important to note that the resulting low-resolution structure compares very well to the trimeric form of PC (Panels B and C of Fig. 5), but not to the hexameric form (Panel A of Fig. 5), and yields an approximately cylindrical structure with a height of 28 Å and a diameter of roughly 100 Å. The latter values are almost identical to those obtained from the initial fits of the PC and PBP –P data (see Table 1).

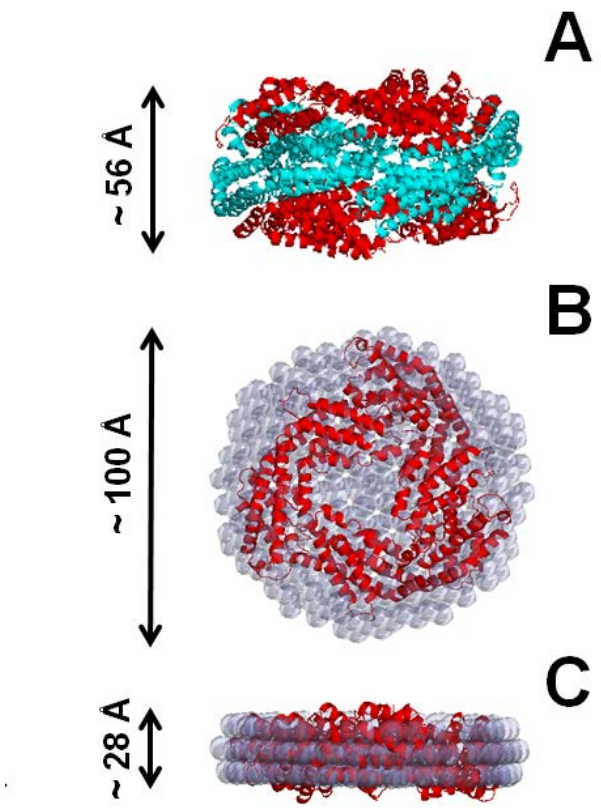

Figure 5. The crystal structures of PC of *Th.elongatus* in hexameric (Panel A) and trimeric form (Panels B and C) based on pdb code 4L1E. The grey spheres in Panels B and C show the low-resolution structure of PC obtained from the SAXS data shown in Fig. 4.

In summary, we can conclude that the SANS data of PBPs of *A.marina* in phosphate buffer (PBP +P) can be well described using a cylindrical form with a length of about 225 Å and a diameter of roughly 100 Å as schematically shown in Panel B of Fig. 5. This finding is qualitatively consistent with earlier electron microscopy studies suggesting a rod-like shape with a length of about 250 [10] or 300 Å [4, 13] as shown in Panel A of Fig. 5. As discussed above, however, SANS data are obtained in buffer solution at room temperature and represent the bulk sample, so that SANS provides information about the sample system under more native conditions than electron microscopy.

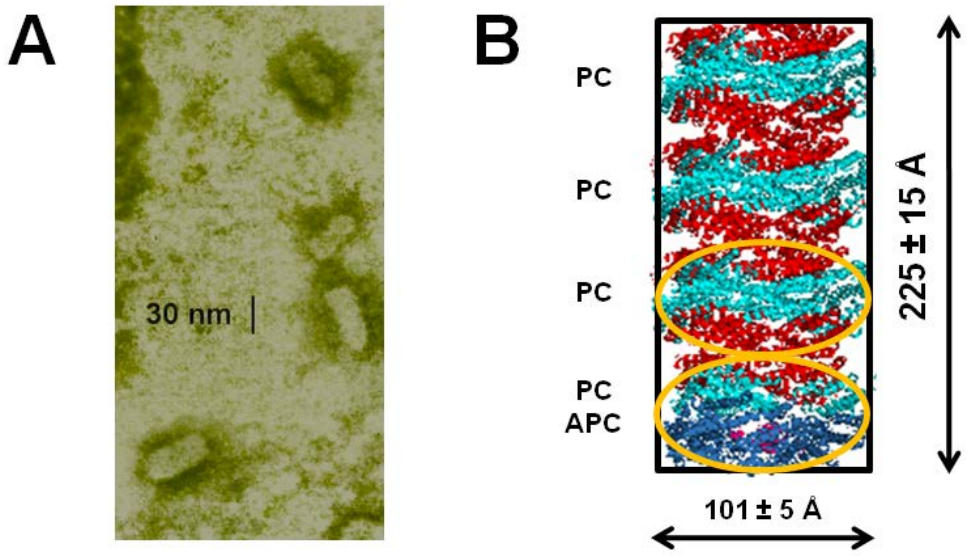

Figure 6. Panel A: electron micrograph of PBPs of *A.marina* in phosphate buffer after negative staining revealing the presence of rod-shaped entities with an approximate length of 30 nm (picture taken from Theiss et al. [13] with permission). Panel B: schematic representation of PBPs of *A.marina* as a cylinder (black rectangle) based on the SANS data of the present study. The crystal structures of seven PC (red and turquoise) trimers (see [31], pdb code 4L1E) and one APC (blue) trimer (see [32], pdb code 1B33) are superimposed on the cylinder structure, see text. The approximate sizes of one PC homodimer and one PC/APC heterodimer are indicated by orange ellipses.

The latter findings permit a reconstruction of the composition of the PBP-rod. The total length of the PBP cylinder of about 225 Å can accommodate 8 trimeric subunits of roughly 28 Å length. Following [4, 10, 13], the trimeric subunit located closest to the reaction center is APC, while all others are PC. It has to be added that the SAXS curves of Fig. 4 can also be modeled by an APC trimer ([32], pdb code 1B33). The resulting structural model for a PBP rod composed of seven PC trimers and one APC trimer (or alternatively 3 PC homo-hexamers plus one PC/APC hetero-hexamer) is schematically shown in Panel B of Fig. 6. Therefore, our SANS/SAXS results corroborate the PBP structural model put forward by [4, 10, 13], however with a more precise length measurement under close to native conditions.

In contrast, the SANS data of PBPs of *A.marina* in MES-buffer lacking phosphate (PBP -P) revealed a splitting of the PBP rods into cylindrical subunits with a radius of 50 Å and a height of 28 Å, but also a pronounced aggregation of the sample. Comparative SAXS and SANS experiments on PC suggest that this subunit may be identical to trimeric PC. It was also verified that trimeric APC would produce roughly the same low-resolution structure (not shown).

The latter structural information can now be used to interpret the different 4.5 K absorption spectra of PBP +P and PBP –P, respectively. Upon phosphate removal, the absorption spectrum of PBP –P showed a slight blue-shift of the main absorption peak to ~631 nm and a more pronounced shoulder at ~645 nm. Further differences among low-energy states were visible in the second derivative spectra. Our SANS data are consistent with a splitting of the PBP rods into PC trimers in phosphate-less samples as inferred before by Theiss et al. [13] based on impaired EET in PBP –P samples. However, also a pronounced aggregation was observed. In principle, the shifts in spectral positions of low-energy states visible in the inset of Fig. 1 may be explained by changes in the protein environment or in the excitonic coupling upon splitting of the PBP rod into trimeric subunits. However, excitonic coupling between chromophores of different trimeric subunits appears to be too weak to have a significant influence on the spectra. Therefore, it is more likely that the additional unspecific aggregation of PBP subunits visible in the SANS data of PBP –P is responsible for the spectral changes visible in Fig. 1, i.e. mainly the slight blue-shift of the main absorption peak and the emergence of the shoulder at ~645 nm. In more general terms, our data also suggest that aggregation affects the positions of PC/APC/PBP low-energy states.

Conclusion

Acknowledgement

Financial Support by the Estonian Science Foundation (Grant No. 9453) and the Estonian Research Council (Grant IUT02-28) is gratefully acknowledged. J. P. is also deeply indebted to the European Social Fund's Internationalisation Programme DoRa for financial support. Furthermore, J.P., and H.-J.E. gratefully acknowledge support from Deutsche Forschungsgemeinschaft (SFB 429, TP A1). We also thank S. Kussin and M. Weß (TU Berlin) for their expert help in sample preparation.

TABLE 1

Fit parameters of SANS and SAXS data

PC subunits Yumo			**PBP Saclay**	
Sample	PC in 5% D_2O	PC in 100% D_2O	PBP –P MES-buffer 100% D_2O	PBP +P Phosphate buffer 100% D_2O
Cylinder				
Scale	6.80 e-4	3.5 e-3	1.69 e-4	9.3 e-5
Radius (Å)	50±5	50±5	50±5	50±5
Length (Å)	28±5	28±5	28±5	225±20
SLD cylinder ($Å^{-2}$)	3.5 e-6	3.5 e-6	3.5 e-6	3.5e-06
SLD solvent ($Å^{-2}$)	-2.2 e-7	6.36 e-6	6.3 e-6	6.36e-06
Power Law				
Amplitude	8 e-5	4 e-4	1.59 e-05	8 e-09
(-)Power	1.84	1.84	3	3
Incoh. bkg	1.2e-06	1.2e-06	0.112	0.113

References

1 Miyashita, H., Ikemoto, H., Kurano, N., Adachi, K., Chihara, M., Miyachi, S. Chlorophyll d as a major pigment, Nature 1996, 383, 402.

2 Chen, M., Quinnell, R. G., Larkum, A. W. D. The major light-harvesting pigment protein of Acaryochloris marina. FEBS Lett. 2002, 514, 149 -152.

3 Chen, M., Bibby, T. S. Photosynthetic apparatus of antenna-reaction centres supercomplexes in oxyphotobacteria: insight through significance of Pcb/IsiA proteins. Photosyn. Res. 2005, 86, 165-173.

4 Marquardt, J., Senger, H., Miyashita, H., Miyachi, S., Mörschel, E. Isolation and characterization of biliprotein aggregates from Acaryochloris marina, a prochloron-like prokaryote containing mainly chlorophyll d. FEBS Lett. 1997, 410, 428-432.

5 Hu, Q., Marquardt, J., Iwasaki, I., Miyashita, N., Kurano, H., Mörschel, E. Miyachi, S., Molecular structure localization and function of biliproteins in the chlorophyll a/d containing oxygenic photosynthetic procaryote Acaryochloris marina, Biochim. Biophys. Acta 1999, 1412, 250-261.

6 Adir, N. Elucidation of the molecular structures of components of the phycobilisome: reconstructing a giant, Photosyn. Res. 2005, 85, 15-32.

7 Mac Coll, R. Allophycocyanin and energy transfer. Biochim Biophys Acta 2004,1657:73–81.

8 Watanabe, M., Ikeuchi, M., Phycobilisome: architecture of a light-harvesting supercomplex, Photosynthesis Research, 2013, 116 (2-3), 265-276.

9 Marquardt, J., Mörschel, E., Rhiel, E., Westerman, M. Ultrastrucutre of Acaryochloris marina, an oxyphotobacterium containing mainly chlorophyll d, Arch. Microbiol. 2000, 174, 181-188.

10 Chen, M., Floetenmeyer, M., Bibby, T. S. Supramolecular organization of phycobiliproteins in the chlorophyll d-containing cyanobacterium Acaryochloris marina, FEBS Lett. 2009, 583, 2535-2539.

11 Theiss, C., Schmitt, F. J., Andree, S., Cardenas-Chavez, C., Wache, K., Fuesers, J., Vitali, M., Wess, M., Kussin, S., Eichler, H. J., Eckert, H.-J. Excitation energy transfer in the phycobiliprotein antenna of Acaryochloris marina studied by transient fs absorption and fluorescence spectroscopy. Photosynthesis: energy from the sun, 14th International Congress on Photosynthesis. Dordrecht :Springer, 2008, p. 339–342.

12 Petrasek, Z., Schmitt, F. J., Theiss, C., Huyer, J., Chen, M., Larkum, A., Eichler, H. J. Kemnitz, K., Eckert, H.-J. Excitation energy transfer from phycobiliprotein to chlorophyll d in intact cells of Acaryochloris Marina studied by time- and wavelength-resolved fluorescence spectroscopy, Photochem. Photobiol. Sci. 2005, 12, 1016-1022.

13 Theiss, C., Schmitt, F.-J., Pieper, J., Nganou, C., Grehn, M., Vitali, M., Olliges, R., Eichler, H. J., Eckert, H.-J. Excitation energy transfer in intact cells and in the phycobiliprotein antennae of the chlorophyll d containing cyanobacterium Acaryochloris marina, J. Plant Physiol. 2011, 168 (12), 1473-1487.

14 Gryliuk et al. J. Phys. Chem. B 2014

15 Jacques, D. A., Trewhella, J. Small-angle scattering for structural biology—Expanding the frontier while avoiding the pitfalls, Protein Science 2010, 19, 2570-2577.

[16] Kikhney, A. G., Svergun, D. I. A practical guide to small angle X-ray scattering (SAXS) of flexible and intrinsically disordered proteins, FEBS Lett. 2015, 589, 642-657.

[17] G. Nagy, G. Garab, J. Pieper, Neutron Scattering in Photosynthesis Research, in: Contemporary Problems of Photosynthesis (Editors: S. Allakhverdiev, A. B. Rubin, V. A. Shuvalov) Izhevsk Institute of Computer Science, Izhevsk–Moscow, 2014, Vol. 1, p. 69–121.

[18] G. Nagy, D. Posselt, L. Kovács, J. K. Holm, M. Szabó, B. Ughy, L. Rosta, J. Peters, P. Timmins, G. Garab, Reversible membrane reorganizations during photosynthesis in vivo: revealed by small-angle neutron scattering, Biochem. J. 436, 2011, 225.

[19] J. J. K. Kirkensgaard, J. K. Holm, J. K. Larsen, D. Possel, Simulation of small-angle X-ray scattering from thylakoid membranes, J. Appl. Crystallogr. 42, 2009, 649.

[20] Pieper, J. et al., Optofluid. 2015, 2, 35-39.

[21] Liberton et al., J. Biol. Chem. 2013, 288, 3632-3640.

[22] Cardoso et al., J.Phys.Chem. 2009, 113, 16377-16383.

[23] Tang, K.-H., Blankenship, R. E., Photosyn. Res. 2012, 111, 205-217.

[24] Chen, M., Bibby, T.S., Nield, J., Larkum, A.W.D., Barber, J. Structure of a large photosystem II supercomplex from Acaryochloris marina, FEBS Lett. 2005, 579, 1306-1310.

[25] Brulet, A. et al., J. Appl. Cryst. 2007, 40, 165-177.

[26] D. I. Svergun, 'Determination of the Regularization Parameter in Indirect-Transform Methods Using Perceptual Criteria', Journal of Applied Crystallography, 25 (1992), 495-503.

[27] Kline S. R., 'Reduction and Analysis of Sans and Usans Data Using Igor Pro', Journal of Applied Crystallography, 39 (2006), 895-900.

[28] D. Franke, and D. I. Svergun, 'Dammif, a Program for Rapid Ab-Initio Shape Determination in Small-Angle Scattering', Journal of Applied Crystallography, 42 (2009), 342-46.

[29] P. V. Konarev, V. V. Volkov, A. V. Sokolova, M. H. J. Koch, and D. I. Svergun, 'Primus: A Windows Pc-Based System for Small-Angle Scattering Data Analysis', Journal of Applied Crystallography, 36 (2003), 1277-82.

[30] D. I. Svergun, C. Barberato, and M. H. J. Koch, 'Crysol -a Program to Evaluate X-Ray Solution Scattering of Biological Macromolecules Form Atomic Coordinates', J. Appl. Cryst., 28 (1995), 768-73.

[31] Singh, N.K., et al., Crystal structure and interaction of phycocyanin with beta-secretase: A putative therapy for Alzheimer's disease. CNS Neurol Disord Drug Targets, 2014. 13(4): p. 691-8.

[32] Reuter, W., et al., Structural analysis at 2.2 A of orthorhombic crystals presents the asymmetry of the allophycocyanin-linker complex, AP.LC7.8, from phycobilisomes of Mastigocladus laminosus. Proc Natl Acad Sci U S A, 1999. 96(4): p. 1363-8.